Highly Sensitive Detection of Infrared Photons by Nondegenerate Two-Photon Absorption Under Midinfrared Pumping

Jianan Fang,[1] Yinqi Wang,[1] Ming Yan,[1] E Wu,[1] Kun Huang,[1,*] and Heping Zeng[1,2,3,4,†]

[1] *State Key Laboratory of Precision Spectroscopy, East China Normal University, Shanghai 200062, China*
[2] *Jinan Institute of Quantum Technology, Jinan, Shandong 250101, China*
[3] *CAS Center for Excellence in Ultra-intense Laser Science, Shanghai 201800, China*
[4] *Shanghai Research Center for Quantum Sciences, Shanghai 201315, China*

(Received 14 October 2020; revised 13 November 2020; accepted 16 November 2020; published 10 December 2020)

We demonstrate highly sensitive photon counting in the infrared region based on two-photon absorption (2PA) in a silicon avalanche photodiode, where the required photon energy for inducing effective conductivity is provided by an intense midinfrared (MIR) field at 3 μm. The used MIR pumping scheme can not only benefit from the enhanced 2PA coefficient in the nondegenerate regime, but also eliminate the detrimental background noises due to the pump harmonic excitation of the pump. Consequently, the enhancement factor for the signal counting rate unprecedentedly reached about 10^5 with input infrared pulses at the femtojoule level. Additionally, the noise equivalent power is substantially improved by 2 orders of magnitude in comparison to conventional schemes with near-infrared pumping. Therefore, the presented configuration might provide an alternative to realize sensitive infrared detection and imaging with desirable features of room-temperature operation, no phase-matching requirement, and broadband responding window, which can find a variety of applications, including remote ranging, sensitive sensing, biochemical imaging, and trace spectroscopy.

DOI: 10.1103/PhysRevApplied.14.064035

I. INTRODUCTION

Sensitive infrared detection plays an enabling role in numerous applications such as laser ranging, optical communication, environmental monitoring, biomedical sensing, and photoluminescence analysis [1,2]. Generally, the sensitivity of infrared detectors is limited by the relatively large dark noise especially at room-temperature operation, which is partially due to the narrow semiconductor bandgap [3]. This issue becomes more conspicuous for optical detectors working at longer infrared wavelengths. Cryogenic operation can help to suppress the thermal radiation and dark current, yet it remains challenging to approach single-photon sensitivity [4,5]. In comparison, high-efficiency and low-noise photon counters are commercially available with silicon-based avalanche photodiodes (SiAPDs) due to their higher bandgap [6]. In this context, the so-called frequency up-conversion technique has recently attracted increasing attention, where the infrared signal is spectrally translated into the visible band before being detected by a high-performance Si detector [7–9].

This simple but effective protocol has mainly been instantiated in two categories. The first one relies on the nonlinear manipulation on the infrared field, such as resorting to sum frequency generation [10–12] and four-wave mixing [13,14]. In this case, a phase-matching condition is typically required to realize efficient parametric interactions, yet usually at the price of a narrow accepted wavelength window [15]. In parallel, the other strategy is based on the material nonlinearity of the detector itself, which specifically involves the manipulation of free charge carriers by two-photon [16,17] or multiphoton [18–20] absorption. The underlying generation and recombination of charge carriers do not require phase matching, thus favoring broadband operation and free of optics alignment [21]. The degenerate two-photon absorption (D2PA) has long been recognized as being useful to detect infrared photons in wide-bandgap semiconductors. For instance, autocorrelators based on 2PA were commonly used to characterize ultrafast infrared pulses in the infrared regions [22]. Recently, extreme nondegenerate 2PA (ND2PA) has been investigated to show a significant enhancement for the absorption coefficient in comparison to the D2PA case [23–26]. Consequently, sensitive midinfrared imaging is demonstrated by using a direct-bandgap GaN photodiode sensor [27] and indirect-bandgap Si CCD camera [28]. Additionally, infrared photon counting has

*khuang@lps.ecnu.edu.cn
†hpzeng@phy.ecnu.edu.cn

been demonstrated based on a GaAs photomultiplier tube (MPT) [29] and a SiAPD [30].

However, in the reported demonstrations, the detector sensitivity is inevitably limited by the D2PA of the intensive pumping field. Although the sensitivity can typically be improved by using the lock-in detection with a modulated signal, the severe pump-induced noise may saturate the detector, thus limiting the dynamic range of the detector [23,28]. To go beyond the demonstrated sensitivity, a lower pump frequency can be chosen to eliminate the severe background noises due to the harmonic excitation of pump photons, whereas the parasitic process of three-photon absorption (3PA) is many orders of magnitude weaker and may be neglected [21,31,32].

Here, we demonstrate highly sensitive detection for infrared photons by ND2PA in a SiAPD under midinfrared (MIR) pumping. The chosen pump wavelength at 3070 nm made the pump photon energy of 0.4 eV much lower than the semiconductor midgap about 0.56 eV, which thus eliminated the D2PA in spite of the high pump intensity. As a result, the residual background noise is mainly ascribed to the negligible three-photon absorption process, which allows us to improve the noise equivalent power by 2 orders of magnitude than that in conventional schemes with near-infrared pumping. Thanks to the substantial suppression of background noise, infrared pulses with femtojoule energy can be identified, which exhibit an enhanced counting rate by a factor closed to 10^5 in comparison to the case of direct detection based on D2PA. Additionally, we experimentally investigate the thermal effect on the 2PA behavior, which shows a degradation of count rates as increasing the MIR pump power. This finding may provide useful guidance to employ the presented configuration of infrared detection in subsequent applications.

II. BASIC PRINCIPLES

The underlying mechanism of the infrared detection scheme is based on absorbing two photons in a semiconductor with a bandgap of E_g. The photon energy of signal and pump fields is $\hbar\omega_1$ and $\hbar\omega_2$. $\hbar\omega_1 + \hbar\omega_2 > E_g$ should be satisfied to generate electro-hole pairs, thus giving rise to a photocurrent. In the nondegenerate scenario, the carrier density has a linear dependence on the pump power. On one hand, efficiency detection requires sufficiently high pump power. On the other hand, intensive pump intensity inevitably induces background noises due to harmonic absorption processes. The trade-off can be mitigated by choosing a lower pump photon energy. For instance, the condition of $\hbar\omega_2 < E_g/2$ excludes the appearance of D2PA for the pump. Consequently, the pump-induced noise is substantially suppressed due to the much weaker 3PA process, hence leading to an enhanced sensitivity of the 2PA-based detector. Furthermore, theoretical investigation has revealed that infrared single-photon detection is possible in a SiAPD if the pump frequency is small enough to avoid the unwanted higher-order absorption processes [21].

Notably, the nondegenerate operation can significantly enhance the nonlinear absorption [23,24]. Specifically, in the scattering matrix formalism with two parabolic bands, the 2PA coefficient α_2 for direct bandgap semiconductors can be written as [33]

$$\alpha_2(\omega_1,\omega_2) = K\frac{\sqrt{E_p}}{n_1 n_2 E_g^3} F_2\left(\frac{\hbar\omega_1}{E_g},\frac{\hbar\omega_2}{E_g}\right), \tag{1}$$

where K is a material-independent constant, E_p is the Kane energy parameter, $n_{1,2}$ are the refractive indices. And the function F_2 is given by

$$F_2(x_1,x_2) = \frac{(x_1+x_2-1)^{3/2}}{2^7 x_1 x_2^2}\left(\frac{1}{x_1}+\frac{1}{x_2}\right)^2, \tag{2}$$

which indicates that dramatically enhanced 2AP is available when either ω_1 or ω_2 becomes small. Note that for an indirect bandgap semiconductor, such as Si, the enhancement behavior has also been observed experimentally [25,26] and theoretically [34].

In our experiment, the pump wavelength is chosen to be 3070 nm for detecting the signal at 1550 nm, which correspond to photon energy of 0.4 and 0.8 eV. The combined photon energy of 1.2 eV exceeds the Si bandgap of 1.12 eV, while the pump photon energy is lower than the semiconductor midgap. In this case, the count rate recorded by a SiAPD can be expressed as

$$N_{\text{total}} = \beta P_1^2 + \gamma P_2^3 + \beta' P_1 P_2, \tag{3}$$

where P_1 and P_2 represent the signal and pump powers. In a practical situation of sensitive detection, the faint signal is typically gated by a strong pump, i.e., $P_1 \ll P_2$. Hence the background noise induced by the pump is reduced to be

$$N_{\text{D3PA}} = \gamma P_2^3, \tag{4}$$

while the effective signal due to the ND2PA is

$$N_{\text{ND2PA}} = \beta' P_1 P_2. \tag{5}$$

As a comparison to the detection scheme based on D2PA of the signal, the enhancement factor G for the resulting count rate can be defined as

$$G = N_{\text{ND2PA}}/N_{\text{D2PA}} = \beta' P_1 P_2/\beta P_1^2 \propto 1/P_1. \tag{6}$$

Indeed, the strong pump field serves as a local oscillator for amplifying the photocurrent, which thus enables detection of extremely weak signals.

III. EXPERIMENTAL SETUP

Figure 1 presents the experimental scheme. The initial light source is from a passively synchronized fiber laser system, which has been detailed in Ref. [35]. The involved YDFL and EDFL are mode locked at a repetition rate of 15.8 MHz to deliver picosecond pulses at 1030 and 1550 nm, respectively. The power of generated pulses is then boosted by Yb- and Er-doped fiber amplifiers (YDFA and EDFA). The amplified dual-color pulses can facilitate the preparation of MIR pulses at 3070 nm by performing difference-frequency generation within a periodically poled lithium niobate (PPLN) crystal. A delay line (Delay1) consisting of two fiber collimators is used to precisely tune the temporal overlap for reaching an optimized conversion efficiency. After a long-pass filter, the spectrally purified MIR light serves as the pump source for implementing the subsequent 2PA-based detector. The other branch from the EDFL is used to prepare the near-infrared (NIR) signal source. The signal and pump powers can be continuously tuned by rotating the half-wave plate (HWP) before the polarization beam splitter (PBS) or the polarizer. Finally, the signal and pump sources are spatially combined by a dichroic mirror before being coupled into a ZrF4 single-mode patch cable (Thorlabs, P3-23Z-FC-1). The fluoride fiber has a high intrinsic transmission above 97% at the two relevant wavelengths. The mixed beam is steered into the a single-photon detector based on SiAPD. The count rate from the detector output is measured by a frequency counter (Tektronix, FCA3100). Note that another delay line (Delay2) is used to determinate the contributions of degenerate and nondegenerate responses [30]. More details about the experiment setup can be found in Appendix A.

IV. RESULTS AND DISCUSSION

Now we turn to characterize the photon-counting performance of the 2PA-based detector. Figure 2(a) presents the relevant transitions within the energy diagram of a silicon detector, which include D2PA at 1550 nm, D3PA at 3070 nm, and ND2PA between them. The corresponding experimental data are shown in Fig. 2(b). The log-log plot shows a linear dependence between the recorded count rate and the input pulse energy. As expected, the fitted slopes for the cases of D2PA, D3PA, and ND2PA are found to be 2, 3, and 1, respectively. Details about the fitting parameters are given in Appendix B. It can be seen that the pump-induced noise due to D3PA is about 6 orders of magnitude lower than that due to D2PA for a given pump power. This observation validates the efficacy of the MIR-pumping approach to enhance the detection sensitivity. Practically, the pump power can be optimized to reach a background noise close to the dark counts, about 100 Hz defined by the Si detector itself. In the two aforementioned scenarios, the allowed power for MIR pumping is about 40 dB higher than that for NIR pumping, thus resulting in a much higher detection efficiency. In Fig. 2(b), an example of the linear response for the ND2PA is given under a MIR pulse energy of 0.32 nJ. The detection floor of about 1 kHz is defined by the pump-induced 3PA noise. As a result, the resolvable signal power can reach the femtojoule level corresponding to about 8×10^3 photons per pulse. It is worth noting that the sensitivity is achieved without the need of lock-in detection. Therefore, the detection speed and dynamic range will be significantly improved by using the presented configuration.

Then we systematically investigate the responding behavior for the ND2PA on the input signal power. In the

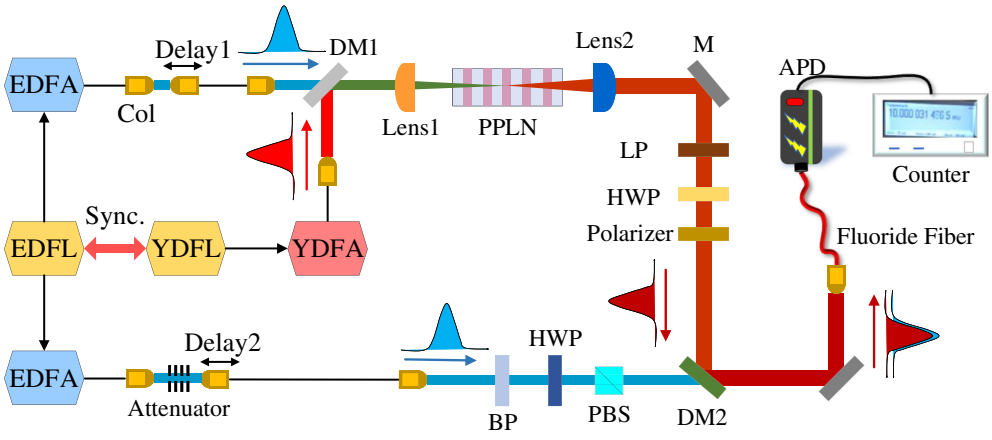

FIG. 1. Schematic of 2PA-based infrared detection based on temporally synchronized fiber lasers. The synchronized pulses at 1030 and 1550 nm originate from two Yb- and Er-doped fiber lasers (YDFL and EDFL), respectively. The pump source at MIR is prepared by the difference-frequency generation between the dual-color beams, while the signal source is obtained after a series of calibrated attenuators. The signal and pump sources are then spatially coupled into a section of fluoride fiber before being detected by a SiAPD. Col, collimator; BP, band-pass filter; LP, long-pass filter; HWP, half-wave plate; PBS, polarization beam splitter; DM, dichroic mirror; PPLN, periodically poled lithium niobate crystal; APD, avalanche photodiode.

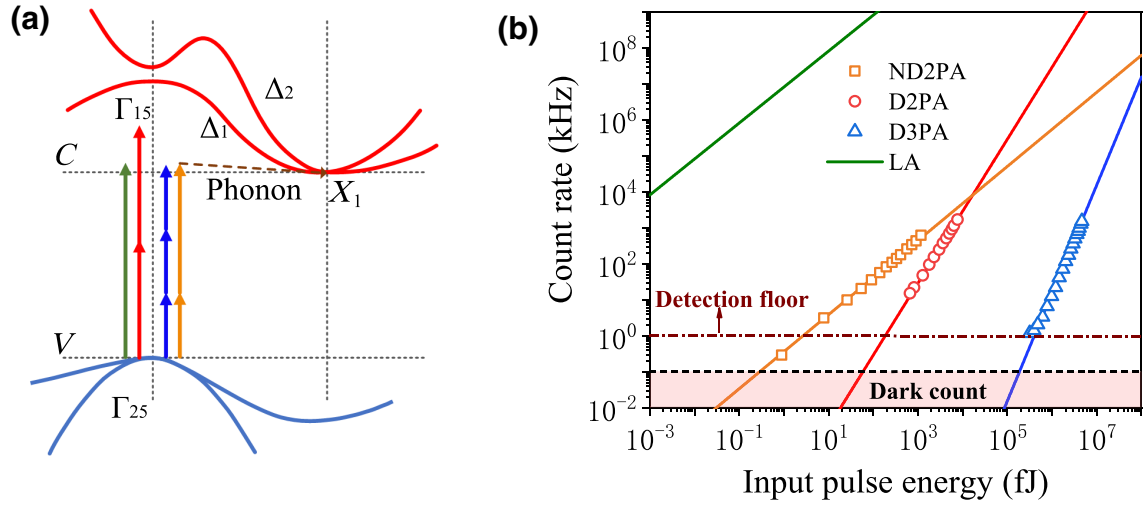

FIG. 2. Highly sensitive infrared photon counting via two-photon absorption under midinfrared pumping. (a) Energy diagram of an indirect bandgap silicon detector. The relevant transitions for comparison include linear absorption (LA) at 1030 nm, D2PA at 1550 nm, D3PA at 3070 nm, and ND2PA. In the presence of intense midinfrared pump, the infrared photon can promote a valence-band electron to a conduction-band state with the help of an intermediate phonon. (b) Recorded count rates by the SiAPD as a function of input pulse energy for various energy-level transitions. Note that the MIR pulse energy at 3070 nm is set at 0.32 nJ for the nondegenerate curve. The dark count of 100 Hz is measured by blocking the injecting light onto the detector. The detection floor about 1 kHz is defined by the noise level with the presence of 0.32-nJ MIR pump pulses.

experiment, the contribution of the ND2PA is identified by the difference between the count rates corresponding to the full overlap and well separation for the signal and pump pulses. Figure 3(a) illustrates the expected linear dependence on the signal pulse energy for various settings of MIR pump power, as predicted by Eq. (5). Also, the count rate increases in the presence of a higher pump power, which implies a higher detection efficiency. Additionally, the ND2PA count rate is greatly amplified due to the presence of the pump in comparison to the D2PA scheme. Following the definition by Eq. (6), the enhancement factor will be inversely proportional to the signal power, as manifested in Fig. 3(b). Thanks to the significant suppression of the pump-induced noise, much lower signal power can be resolved. Consequently, an unprecedented enhancement factor about 6×10^4 is obtained for a signal pulse energy of 1 fJ under a 40-mW pump, thus showing a hundredfold improvement over previous demonstrations [28–30], as listed in Appendix C.

In the following, we proceed to investigate the evolution of ND2PA count rate as a function of the MIR pump power. According to Eq. (5), the count rate should be linearly proportional to the pump power. However, the expected linear dependence is only confirmed in the low-power pumping regime as shown in Fig. 4(a). Under higher pump powers, the count rate tends to be saturated before starting to decrease dramatically. This phenomenon might be related to the thermal effect due the intensive MIR radiation. Indeed, we experimentally observe that the count rate slowly decreases to a stabilized value when the pump is launched. Empirically, the ND2PA coefficient β' can be expanded in a Taylor series as $\beta' = \beta'^{(0)} + \beta'^{(1)}P_2$. The resulting expression of count rate due the ND2PA is given by $N_{\mathrm{ND2PA}} = P_1[\beta'^{(0)}P_2 + \beta'^{(1)}P_2^2]$. Furthermore, identical behavior exhibited for the measured count rate due to D2PA. In this case, the signal and pump pulses are temporally separated in order to exclude the nonlinear interaction between them. Similarly, the D2PA coefficient β can be expanded as $\beta = \beta^{(0)} + \beta^{(1)}P_2$, which results in a count rate $N_{\mathrm{D2PA}} = P_1^2[\beta^{(0)} + \beta^{(1)}P_2]$. The inhibiting effect due to the MIR pumping can be quantitatively characterized by $\Delta N_{\mathrm{D2PA}} = \beta^{(1)}P_2P_1^2$. As given in Fig. 4(b), the decrement of the D2PA count rate for the signal is indeed more pronounced as augmenting the pump power. Further studies show that this inhibiting phenomenon can also be observed for single-photon absorption at 1030 nm and three-photon absorption at 3070 nm. A possible reason may lie in the slight variation of the optimal value for the reverse-biased voltage in the presence of the non-negligible heat on the APD chip. Since the APD is operated in the Geiger mode, the photon-counting performance is usually sensitive to the change of the reverse-biased voltage. Our observations here may stimulate further theoretical and experimental investigations to unveil the underlying mechanism.

Finally, we analyze the noise equivalent power (NEP), which is a useful figure of merit for characterizing the sensitivity of optical detectors. It is desirable to have an NEP as low as possible, which corresponds to a lower noise floor and hence a more sensitive detector. Particularly, the NEP for a photon counter is typically defined as [9]

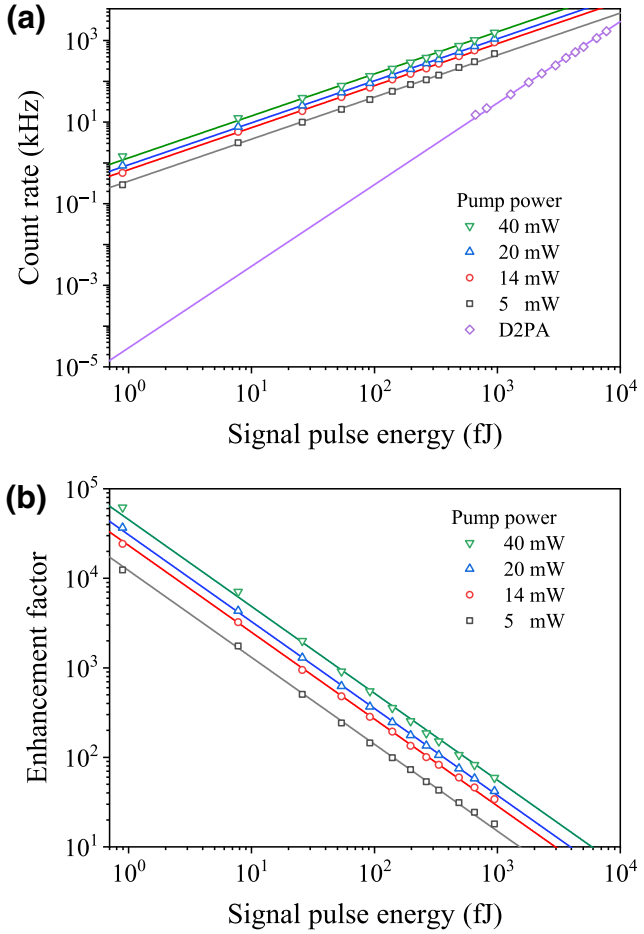

FIG. 3. Near-infrared detection performance based on the ND2PA in the presence of different pump powers. (a) Count rate for the ND2PA increases linearly with the input pulse energy. For comparison, D2PA for the infrared signal is also included, which indicates a significant enhancement on the detection efficiency. (b) Enhancement factor for the recorded count rates due to ND2PA effect with a comparison to the detection scheme based on the D2PA of the signal alone.

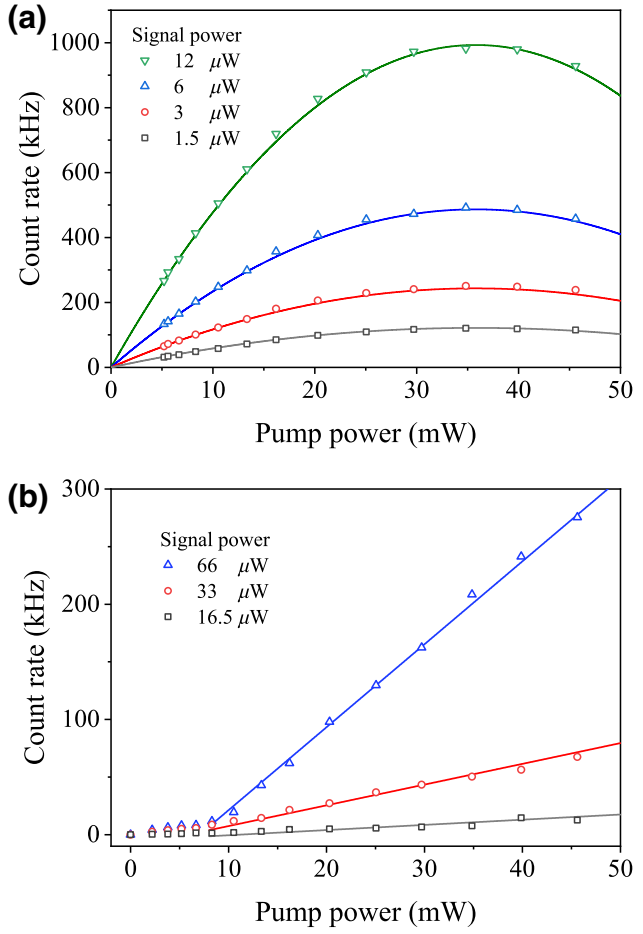

FIG. 4. (a) Count rates for the ND2PA vary as the MIR pump power for various settings of signal power. The solid lines are given by the theoretical model in the text, where the dependence of the absorption coefficient on the pumping power is taken into account. (b) Decrement of count rates for the D2PA at 1550 nm with increasing the MIR pump power. Note that the signal and MIR pulses are temporally separated for performing this measurement.

$\mathcal{N} = h\nu\sqrt{2N_b}/\eta$, where $h\nu$ represents the signal photon energy, N_b denotes the background count rate, and η is the detection efficiency. For a 2PA-based detector, η is given by the ratio between the detected count rate N_{ND2PA} and input photon flux N_1: $\eta = N_{\mathrm{ND2PA}}/N_1 = \beta' P_1 P_2/P_1/h\nu = \beta' P_2 h\nu$. And N_b is comprised of the dark noise N_0 of the SiAPD and the pump-induced noise: $N_b^{\mathrm{MIR}} = N_0 + \gamma P_2^3$ and $N_b^{\mathrm{NIR}} = N_0 + \beta P_2^2$, which correspond to MIR and NIR pumping, respectively. Therefore, the expressions of NEP for the two cases are given by

$$\mathcal{N}^{\mathrm{MIR}} = \frac{\sqrt{2(N_0 + \gamma P_2^3)}}{\beta' P_2}, \qquad \mathcal{N}^{\mathrm{NIR}} = \frac{\sqrt{2(N_0 + \beta P_2^2)}}{\beta' P_2}. \tag{7}$$

At the weak-pumping condition of $P_2 \to 0$, the background noise is dominated by the detector dark noise, which leads to $\mathcal{N} \propto P_2^{-1}$. At the other extreme condition with $P_2 \to +\infty$, $\mathcal{N}^{\mathrm{MIR}} \propto P_2^{1/2}$ and $\mathcal{N}^{\mathrm{NIR}}$ approaches to be constant. These evolutions are illustrated in Fig. 5, which indicates a significant improvement of NEP under MIR pumping by 2 orders of magnitude. Note that the wavelength in the NIR-pumping scenario is set to 1550 nm. Actually, other wavelengths below 2200 nm will be expected to exhibit similar behavior, albeit with tolerable deviations. The parameters used in the simulation are obtained from the fitted values for the experimental data shown in Figs. 3 and 4.

It is worth noting that the MIR-pumping strategy should, in principle, be applicable for broadband sensitive detection at the infrared region. For instance, wavelengths up

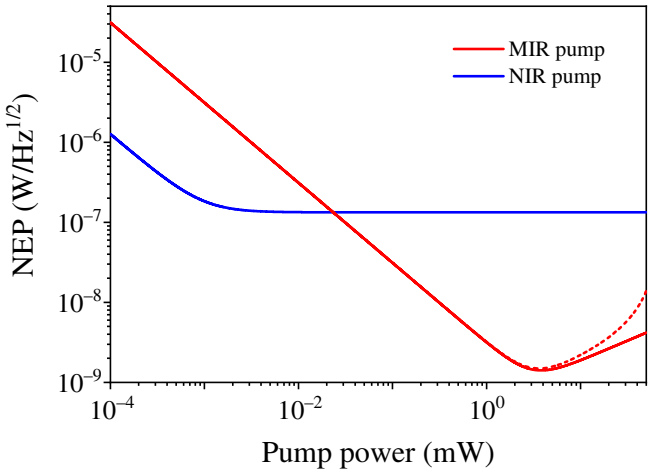

FIG. 5. Noise equivalent power as a function of the pump strength in the cases of using two typical pump wavelengths at 3070 and 1550 nm. Comparatively, much lower NEP can be obtained in the MIR-pumping scenario. Note that the dashed line represents the model by including the thermal effect due the strong pump intensity.

to 1.7 μm are applicable for the operational MIR pump at 3 μm. Furthermore, a spectrum over 1.2–2 μm can be covered with an adapted pump wavelength of about 2.4 μm. This particular wavelength can be readily accessed by MIR lasers based on Cr^{2+}:Zn-Se or Cr^{2+}:Zn-S [36]. In our presented configuration, the high overall detection efficiency requires synchronous pump pulses. The adopt of continuous-wave pump allows us to implement passive detection of signal photons. To approach a comparable detection efficiency, the average pump power should be much higher than that in the pulsed scenario, which may surpass the damage threshold of the optical detector. This limitation might be mitigated by resorting to the waveguide geometry or microcavity structure [25,26], where the light intensity can be boosted by the tight spatial confinement.

V. CONCLUSION

In summary, we demonstrate sensitive infrared detection in the SiAPD using ND2PA based on a MIR-pumping scheme. In this nondegenerated regime, the improvement of nonlinear absorption coefficient for the signal and the elimination of second-harmonic noises of the pump enable us to increase the detection efficiency and reduce the background noise. Consequently, femtojoule-level pulse energy can be identified, which represents a record sensitivity for 2PA-based detectors. The corresponding enhancement factor of the ND2PA count rate unprecedentedly reached about 10^5 in comparison to the scheme based on D2PA.

To go beyond the achieved sensitivity, lower pump photon energy can be employed with a MIR wavelength over 3300 nm. The 3PA noise might thus be removed, which holds potential to ultimately realize single-photon sensitivity as theoretically predicted [21]. Furthermore, the detection performance will also be enhanced by using waveguide geometry or microcavity structure with the help of the tight spatial confinement and long nonlinear interaction length [25,26]. It is worth noting that the efficacy of our implemented configuration can immediately facilitate sensitive infrared imaging via a Si electron-multiplying CCD, thus favoring desirable features of high spatial resolution and high-speed frame rate. Additionally, the gated detection by pulsed pumping provides a high-precision temporal resolution for sensitive infrared detection and imaging, which may be useful for relevant applications, such as time-resolved molecular spectroscopy and dynamic photoluminescence analysis.

ACKNOWLEDGMENTS

This work is supported by National Key Research and Development Program (Grant No. 2018YFB0407100), Science and Technology Innovation Program of Basic Science Foundation of Shanghai (Grant No. 18JC1412000), Program for Professor of Special Appointment (Eastern Scholar) at Shanghai Institutions of Higher Learning, National Natural Science Foundation of China (Grants No. 11621404 and No. 11727812), Shanghai Municipal Science and Technology Major Project (Grant No. 2019SHZDZX01).

APPENDIX A: EXPERIMENTAL SETUP

The whole experimental setup mainly consists of three parts, corresponding to realizing synchronized fiber lasers, preparing signal and pump sources, and implementing 2PA-based detection. The synchronized laser system is based on the Er-doped and Yb-doped fiber lasers in a master-slave layout. The master pulses at 1550 nm are injected into the laser cavity of the YDFL based on a nonlinear amplifying loop mirror (NALM). The induced periodic nonreciprocal phase shift via the cross-phase modulation effect within the NALM initiated the synchronous mode locking of the slave laser, which results in a passive locking of the relative repetition rates between the two lasers [35].

The pulse durations of the YDFL and EDFL are measured to be 36 and 5 ps by using an autocorrelator (APE, pulseCheck SM). The relative timing jitter is measured to be about 20 fs, which is negligible comparing to the pulse duration. In order to prepare the midinfrared pump source, we perform difference-frequency generation in a PPLN crystal. The pulse duration of the generated MIR field is inferred to be 5 ps from the cross-correlation trace as given in Fig. 6. Then a long-pass filter with a cut-off wavelength of 2.4 μm is used to remove the near-infrared fields. The MIR power can be varied by using a combination of a nanoparticle linear film polarizer (Thorlabs,

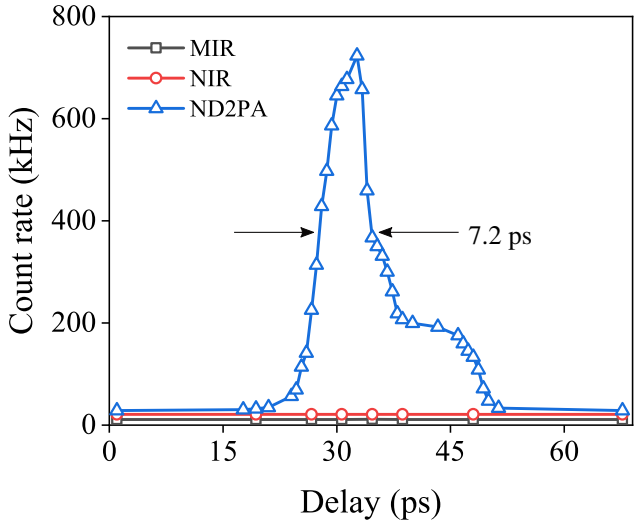

FIG. 6. Measured cross-correlation trace between the signal at 1550 nm and the pump at 3070 nm. The background due to D2PA and D3PA is recorded by solely injecting either the NIR or MIR light.

LPNIRA050) and low-order half-wave plate (Thorlabs, WPLH05M-2940), which serves as the pump source for the subsequent 2PA detection.

In parallel, the signal source is from the attenuated light at 1550 nm. The near-infrared signal is filtered by a band-pass filter centered at 1550 nm with a bandwidth of 40 nm. A delay line is inserted into signal path to temporally tune the overlap between the dual-color pulses. Then, the signal and pump sources are spatially combined by a dichroic mirror before being coupling into a fluoride single-mode fiber. The coupling efficiencies for both beams are about 45%. Both beams are finally detected by a commercial APD detector (Excelitas, SPCM-AQRH-54-FC). By taking into account the 180-μm diameter of the active area for the SiAPD, the average pump power of 35 mW for achieving a peak detection efficiency is corresponding to the intensity of 1.7 MW/cm^2. Note that the commercial APD sensor is optimized for visible wavelengths, the actual pump intensity on the active area will be lower. The light intensity of the signal at the femtojoule level is about 0.8 W/cm^2 at the detector.

APPENDIX B: FITTED PARAMETERS

The parameters for modeling the experimental data is summarized in Table I. Specifically, the D2PA and D3PA coefficients are obtained from the quadratic and cubit fittings as shown in Fig. 7.

TABLE I. Fitted parameter for the involved 2PA and 3PA processes within a SiAPD.

$\beta^{(0)}$ [Hz/W^2]	$\beta^{(1)}$ [Hz/W^3]	$\beta'^{(0)}$ [Hz/W^2]	$\beta'^{(1)}$ [Hz/W^3]	γ [Hz/W^3]
1.12×10^{14}	-1.65×10^{15}	4.53×10^{12}	-6.33×10^{13}	3.59×10^{9}

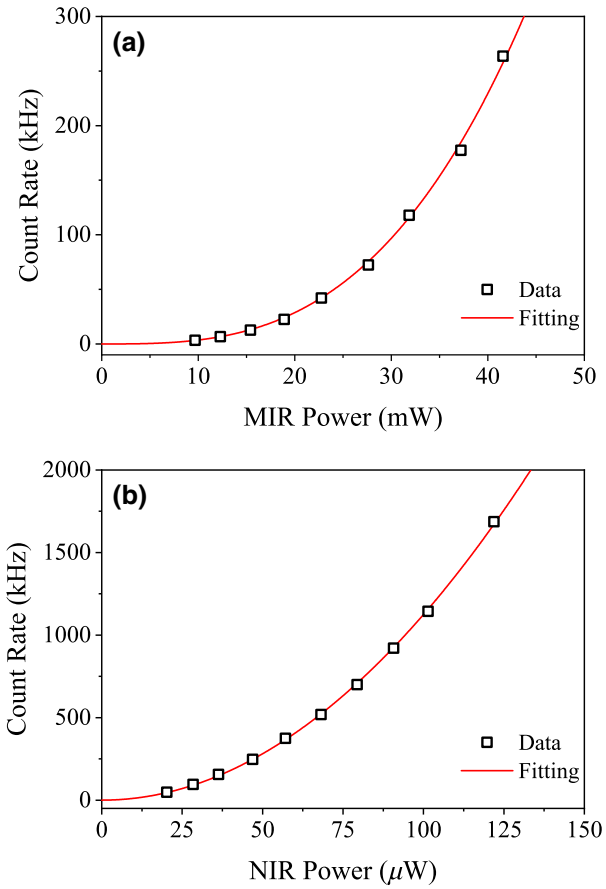

FIG. 7. Count rates as a function of the used power for the MIR-pumping (a) and NIR-pumping (b) scenarios. The fitted lines are used to estimate the values of β and γ for D2PA and D3PA processes in the SiAPD.

Based on the these fitting parameters, the peak detection efficiency of the implemented detector based on ND2PA is given by $\eta_{\mathrm{ND2PA}} = \beta' P_2 h\nu = 1.04 \times 10^{-8}$ in the presence of 35-mW pump power. However, the minimum NEP is optimized at the pump power of 4 mW, leading to $\mathcal{N}^{\mathrm{MIR}} = \sqrt{2(N_0 + \gamma P_2^3)}/\beta' P_2 = 1.4 \times 10^{-9}$ W/Hz$^{1/2}$.

APPENDIX C: PERFORMANCES FOR COMPARISON

As shown in Table II, we list related works on 2PA-based detection for direct comparison. It can be seen that the ND2PA based on MIR pumping favors enhancing the detection sensitivity performance. In Ref. [28], the degenerate background noise due the pump should be subtracted to reveal the signal contribution. Since the noise is much larger than the signal, long acquisition time at the second scale is typically needed to improve the detection

TABLE II. Comparison of passive synchronization performance for mode-locked fiber lasers with comparable pulse durations. λ_s and λ_s indicate the employed signal and pump wavelengths. The photon energy of the pump and the bandgap of the detector are denoted as E_p and E_g, respectively. $E_{\min}$ represents the minimum detectable energy. $G_{\max}$ is the peak enhancement factor for the ND2PA in comparison to the detection based on D2PA.

Ref.	λ_s (μm)	λ_p (μm)	E_p (eV)	Detector	E_g (eV)	$E_{\min}$ (fJ)	$G_{\max}$
This work	1.55	3.07	0.4	Si	1.12	1	6×10^4
[23]	5.6	0.39	3.19	GaN	3.28	10^{6a}	10^3
[28]	3.39	1.48	0.84	Si	1.12	200	10
[29]	1.55	1.9	0.65[b]	GaAs	1.42	10^{7a}	300
[30]	1.85	1.55	0.8	Si	1.12	16	20

[a]These experiments are operated with a continuous-wave signal input.
[b]Although the pump photon energy is below the midgap of the Ga-As detector, the 2PA noise due to pump is dominated in the experiment.

sensitivity. In contrast, the pump-induced noise is substantially suppressed in our configuration, which enables us to identify the weak signal in the presence of the pump. Therefore, a high sensitivity can be obtained here within a much shorter average time, which will be essential for implementing infrared imaging at a fast frame rate. In our experiment, the acquisition time is typically set at 1 ms. Longer average time leads to even lower resolvable signal energy.

[1] M. D. Eisaman, J. Fan, A. Migdall, and S. V. Polyakov, Invited review article: Single-photon sources and detectors, Rev. Sci. Instrum. **82**, 071101 (2011).

[2] J. Zhang, M. A. Itzler, H. Zbinden, and J.-W. Pan, Advances in InGaAs/InP single-photon detector systems for quantum communication, Light Sci. Appl. **4**, e286 (2015).

[3] A. Rogalski, P. Martyniuk, and M. Kopytko, Challenges of small-pixel infrared detectors: A review, Rep. Prog. Phys. **79**, 046501 (2017).

[4] U. Adiyan, T. Larsen, J. José Zárate, L. Guillermo Villanueva, and H. Shea, Shape memory polymer resonators as highly sensitive uncooled infrared detectors, Nat. Comm. **10**, 4518 (2019).

[5] B. Korzh *et al.*, Demonstration of sub-3 ps temporal resolution with a superconducting nanowire single-photon detector, Nat. Photon. **14**, 250 (2020).

[6] R. H. Hadfield, Single-photon detectors for optical quantum information applications, Natrue Photon. **3**, 696 (2009).

[7] J. Huang and P. Kumar, Observation of Quantum Frequency Conversion, Phys. Rev. Lett. **68**, 2153 (1992).

[8] S. Tanzilli, W. Tittel, M. Halder, O. Alibart, P. Baldi, N. Gisin, and H. Zbinden, A photonic quantum information interface, Nature **437**, 116 (2005).

[9] W. Kang, B. Li, Y. Liang, Q. Hao, M. Yan, K. Huang, and H. Zeng, Coincidence-pumping upconversion detector based on passively synchronized fiber laser system, IEEE Photon. Tech. Lett. **32**, 184 (2020).

[10] J. S. Pelc, L. Ma, C. R. Phillips, Q. Zhang, C. Langrock, O. Slattery, X. Tang, and M. M. Fejer, Long-wavelength-pumped up-conversion single-photon detector at 1550 nm: Performance and noise analysis, Opt. Express **19**, 21445 (2011).

[11] K. Huang, X. Gu, H. Pan, E. Wu, and H. Zeng, Few-photon-level two-dimensional infrared imaging by coincidence frequency upconversion, Appl. Phys. Lett. **100**, 151102 (2012).

[12] A. Barh, P. J. Rodrigo, L. Meng, C. Pedersen, and P. Tidemand-Lichtenberg, Parametric upconversion imaging and its applications, Adv. Opt. Photon. **11**, 952 (2019).

[13] H. J. McGuinness, M. G. Raymer, C. J. McKinstrie, and S. Radic, Quantum Frequency Translation of Single-Photon States in a Photonic Crystal Fiber, Phys. Rev. Lett. **105**, 093604 (2010).

[14] Q. Li, M. Davanço, and K. Srinivasan, Efficient and low-noise single-photon-level frequency conversion interfaces using silicon nanophotonics, Nature Photon. **10**, 406 (2016).

[15] M. Mrejen, Y. Erlich, A. Levanon, and H. Suchowski, Multicolor time-resolved upconversion imaging by adiabatic sum frequency conversion, Laser Photon. Rev. **2020**, 2000040 (2020).

[16] A. D. Bristow, N. Rotenberg, and H. M. van Driel, Two-photon absorption and Kerr coefficients of silicon for 850–2200 nm, Appl. Phys. Lett. **90**, 191104 (2007).

[17] M. Reichert, A. L. Smirl, G. Salamo, D. J. Hagan, and E. W. Van Stryland, Observation of Nondegenerate Two-Photon Gain in GaAs, Phys. Rev. Lett. **117**, 073602 (2016).

[18] W. C. Hurlbut, Y.-S. Lee, K. Vodopyanov, P. Kuo, and M. Fejer, Multiphoton absorption and nonlinear refraction of GaAs in the mid-infrared, Opt. Lett. **32**, 668 (2007).

[19] S. Pearl, N. Rotenberg, and H. M. van Driel, Three photon absorption in silicon for 2300–3300 nm, Appl. Phys. Lett. **93**, 131102 (2008).

[20] A. Nevet, A. Hayat, and M. Orenstein, Ultrafast three-photon counting in a photomultiplier tube, Opt. Lett. **36**, 725 (2011).

[21] A. Hayat, P. Ginzburg, and M. Orenstein, Infrared single-photon detection by two-photon absorption in silicon, Phys. Rev. B **77**, 125219 (2008).

[22] D. L. Boiko, A. V. Antonov, D. I. Kuritsyn, A. N. Yablonskiy, S. M. Sergeev, E. E. Orlova, and V. V. Vaks, Mid-infrared two photon absorption sensitivity of commercial detectors, Appl. Phys. Lett. **111**, 171102 (2017).

[23] D. A. Fishman, C. M. Cirloganu, S. Webster, L. A. Padilha, M. Monroe, D. J. Hagan, and E. W. Van Stryland, Sensitive mid-infrared detection in wide-bandgap semiconductors using extreme non-degenerate two-photon absorption, Nat. Photon. **5**, 561 (2011).

[24] C. M. Cirloganu, L. A. Padilha, D. A. Fishman, S. Webster, D. J. Hagan, and E. W. Van Stryland, Extremely nondegenerate two-photon absorption in direct-gap semiconductors [Invited], Opt. Express **19**, 22951 (2011).

[25] N. Poulvellarie, C. Ciret, B. Kuyken, F. Leo, and S.-Pierre Gorza, Highly Nondegenerate two-Photon Absorption in Silicon Wire Waveguides, Phys. Rev. Appl. **10**, 024033 (2018).

[26] Y. Zhang, C. Husko, S. Lefrancois, I. H. Rey, T. F. Krauss, J. Schröder, and B. J. Eggleton, Non-degenerate two-photon absorption in silicon waveguides: Analytical and experimental study, Opt. Express **23**, 17101 (2015).

[27] H. S. Pattanaik, M. Reichert, D. J. Hagan, and E. W. Van Stryland, Three-dimensional IR imaging with uncooled GaN photodiodes using nondegenerate two-photon absorption, Opt. Express **24**, 1196 (2016).

[28] D. Knez, A. M. Hanninen, R. C. Prince, E. O. Potma, and D. A. Fishman, Infrared chemical imaging through non-degenerate two-photon absorption in silicon-based cameras, Light Sci. Appl. **9**, 125 (2020).

[29] F. Boitier, J.-B. Dherbecourt, A. Godard, and E. Rosencher, Infrared quantum counting by nondegenerate two photon conductivity in GaAs, Appl. Phys. Lett. **94**, 081112 (2009).

[30] G. Xu, X. Ren, Q. Miao, M. Yan, H. Pan, X. Chen, G. Wu, and E. Wu, Sensitive infrared photon counting detection by nondegenerate two-photon absorption in si APD, IEEE Photon. Tech. Lett. **31**, 1944 (2019).

[31] T. Wang, N. Venkatram, J. Gosciniak, Y. Cui, G. Qian, W. Ji, and D. Tan, Multi-photon absorption and third-order nonlinearity in silicon at mid-infrared wavelengths, Opt. Express **21**, 32192 (2013).

[32] S. Benis, C. M. Cirloganu, N. Cox, T. Ensley, H. Hu, G. Nootz, P. D. Olszak, L. A. Padilha, D. Peceli, M. Reichert, S. Webster, M. Woodall, D. J. Hagan, and E. W. Van Stryland, Three-photon absorption spectra and bandgap scaling in direct-gap semiconductors, Optica **7**, 888 (2020).

[33] M. Sheik-Bahae, D. C. Hutchings, D. J. Hagan, and E. W. Van Stryland, Dispersion of bound electron nonlinear refraction in solids, IEEE J. Quan. Electron. **27**, 1296 (1991).

[34] N. Cox, D. J. Hagan, and E. W. Van Stryland, in *Proceeding of SPIE 10916, Ultrafast Phenomena and Nanophotonics XXIII*, 1091613 (San Francisco, United States, 2019).

[35] J. Zeng, B. Li, Q. Hao, M. Yan, K. Huang, and H. Zeng, Passively synchronized dual-color mode-locked fiber lasers based on nonlinear amplifying loop mirrors, Opt. Lett. **44**, 5061 (2019).

[36] J. Ma, Z. Qin, G. Xie, L. Qian, and D. Tang, Review of mid-infrared mode-locked laser sources in the 2.0 μm–3.5 μm spectral region, Appl. Phys. Rev. **6**, 021317 (2019).